

# Chemical Science

Volume 12  
Number 38  
14 October 2021  
Pages 12503–12852

rsc.li/chemical-science



ISSN 2041-6539

**EDGE ARTICLE**

Lauren Takahashi, Toshiaki Taniike, Keisuke Takahashi *et al.*  
Constructing catalyst knowledge networks from catalyst big data in oxidative coupling of methane for designing catalysts

Cite this: *Chem. Sci.*, 2021, 12, 12546 All publication charges for this article have been paid for by the Royal Society of Chemistry

# Constructing catalyst knowledge networks from catalyst big data in oxidative coupling of methane for designing catalysts†

Lauren Takahashi,<sup>a</sup> Thanh Nhat Nguyen,<sup>b</sup> Sunao Nakanowatari,<sup>b</sup> Aya Fujiwara,<sup>b</sup> Toshiaki Taniike<sup>\*b</sup> and Keisuke Takahashi<sup>†\*</sup>

Designing high performance catalysts for the oxidative coupling of methane (OCM) reaction is often hindered by inconsistent catalyst data, which often leads to difficulties in extracting information such as combinatorial effects of elements upon catalyst performance as well as difficulties in reaching yields beyond a particular threshold. In order to investigate C<sub>2</sub> yields more systematically, high throughput experiments are conducted in an effort to mass-produce catalyst-related data in a way that provides more consistency and structure. Graph theory is applied in order to visualize underlying trends in the transformation of high-throughput data into networks, which are then used to design new catalysts that potentially result in high C<sub>2</sub> yields during the OCM reaction. Transforming high-throughput data in this manner has resulted in a representation of catalyst data that is more intuitive to use and also has resulted in the successful design of a myriad of catalysts that elicit high C<sub>2</sub> yields, several of which resulted in yields greater than those originally reported in the high-throughput data. Thus, transforming high-throughput catalytic data into catalyst design-friendly maps provides a new method of catalyst design that is more efficient and has a higher likelihood of resulting in high performance catalysts.

Received 10th August 2021  
Accepted 27th August 2021

DOI: 10.1039/d1sc04390k

rsc.li/chemical-science

## Introduction

The introduction of catalyst informatics has innovated how catalysts are designed and understood based on the trends and patterns that lie within catalyst data.<sup>1–3</sup> Catalyst informatics requires consistent and diverse catalyst data, which is becoming more readily available due to developments in catalysis-centered high throughput experiments which are able to produce such series of consistent catalyst big data.<sup>4–6</sup> While machine learning and data mining have been proven to be effective for extracting knowledge from catalyst data, they are fundamentally limited to expressing the information that is provided by catalyst big data.<sup>7–13</sup> In particular, it is challenging to design descriptors for representing catalysts during machine learning as catalytic performance is strongly coupled with structural features induced by the interaction of chemical elements in catalysts.<sup>14–16</sup> In other words, certain chemical elements might have high catalytic performance; however,

catalytic performance often increases or decreases depending on how such chemical elements combine with other chemical elements.<sup>17</sup> Such combinatorial effects are difficult to design as descriptors, thereby still requiring representation of the combination effect of catalysts within catalyst big data. Here, graph theory is proposed as a means to represent the information and knowledge found within catalyst big data where the relationships within catalyst data are represented as complex networks.<sup>18</sup> Doing so would thus assist in revealing the underlying knowledge in catalyst big data in a comprehensive manner, leading towards a more informed way of designing catalysts.

Catalyst big data for oxidative coupling of methane (OCM) is investigated where OCM aims to directly convert CH<sub>4</sub> to C<sub>2</sub>H<sub>4</sub> and C<sub>2</sub>H<sub>6</sub>.<sup>19,20,23</sup> Big data focused on OCM catalysts are previously collected using high throughput experiments where the dataset consists of 291 catalysts with experimental conditions that result in maximum catalytic performance.<sup>4,5</sup> If the relationships between chemical element combinations in catalysts and experimental conditions as well as catalytic performance are uncovered, it becomes possible to find key combinations for chemical elements and corresponding experimental conditions that result in high C<sub>2</sub> yields. Here, the relationships within the OCM catalyst big data are expanded into networks that provide a basis for designing and understanding the OCM reaction from complex networks.

<sup>a</sup>Department of Chemistry, Hokkaido University, North 10, West 8, Sapporo 060-8510, Japan. E-mail: lauren.takahashi@sci.hokudai.ac.jp; keisuke.takahashi@sci.hokudai.ac.jp

<sup>b</sup>Graduate School of Advanced Science and Technology, Japan Advanced Institute of Science and Technology, 1-1 Asahidai, Nomi, Ishikawa 923-1292, Japan. E-mail: taniike@jaist.ac.jp

† Electronic supplementary information (ESI) available. See DOI: 10.1039/d1sc04390k



## Methodology

The dataset used in this study is a collection of the OCM data for 291 quaternary catalysts represented by M1–M2–M3/support.<sup>5</sup> It has two important features that few other catalyst datasets possess. The first feature is the consistency, which arises from the fact that the catalysts were prepared and evaluated by the exactly same methods. When datasets consist of catalyst data collected from multiple references, data inconsistency due to discrepancies in catalyst preparation and evaluation methods is a major obstacle. There are few datasets of this scale that are collected in a consistent manner, and this was achieved through high-throughput experimentation.<sup>4,5</sup> The second feature is that these 291 catalysts are randomly selected from 36 540 compositions that can be created by combining 28 elements and 9 oxides. The frequency of appearance of individual elements and supports is uniform, without any biases toward known effective compositions, *i.e.* free of sampling bias. The performance of a catalyst as part of a chemical process is sensitive to reaction conditions. Evaluation under specific conditions tends to favor the catalyst that is best suited to those conditions rather than the catalyst that is truly superior. In this dataset, each catalyst is evaluated under 135 reaction conditions with different temperatures and gas compositions, and the data points with the best C<sub>2</sub> yield are extracted and collected.

## Experimental details

Validation experiments are performed on the catalysts proposed from the analysis of network information. The methods of catalyst preparation and evaluation are exactly the same as those used to create the original dataset.<sup>5</sup> Briefly, catalysts are prepared based on a wet impregnation method: a specified support (1.0 g) is loaded with precursors of the elements specified as M1–M3 (0.37 mmol for each), followed by drying and calcination at 1000 °C to obtain a catalyst. Support materials and precursors used are the same as those described in the literature.<sup>5</sup> The OCM performance of the catalysts is acquired using a high-throughput screening instrument developed by some of us.<sup>4,5</sup> The instrument automatically acquires the performance of 20 catalysts under a pre-programmed set of reaction conditions in a fixed-bed flow reactor configuration. Catalyst beds consist of quartz reaction tubes with an inner diameter of 4.0 mm filled with catalyst powder at a bed height of 10 mm. A gas mixture of a specified composition is simultaneously flowed through 20 catalyst beds heated at a specified temperature, and the composition of the effluent gas is measured using a quadrupole mass spectrometer (QMS) equipped with an auto-sampling system. The catalyst performance is obtained for 135 reaction conditions differing in the temperature and feed volume of CH<sub>4</sub>, O<sub>2</sub>, and Ar, where Ar serves as a carrier gas as well as an internal standard in QMS. As in the original dataset, the data point corresponding to the best C<sub>2</sub> yield out of the 135 conditions is extracted, which represents the performance of a catalyst.

## Graph theory

Networks of the created datasets are constructed *via* Gephi.<sup>21</sup> Data from the dataset are extracted and preprocessed to account for graph nodes, edges, and edge weights. Here, graph nodes are objects that represent the catalysts, catalyst supports, corresponding experimental conditions, and the resulting C<sub>2</sub> yields when tested *via* high throughput experiments. Edges represent the connections shared between two nodes while the edge weight is set to 1. In particular, the following data are extracted for network analysis: atomic elements, catalyst supports, C<sub>2</sub> yields of the individual catalysts, C<sub>2</sub> yield groups (0–8%, 8–12%, and 12+%), CH<sub>4</sub>/O<sub>2</sub> ratio (2, 4, and 6), CH<sub>4</sub> flow, O<sub>2</sub> flow, Ar flow, and temperature (700 °C, 750 °C, 800 °C, 850 °C, and 900 °C). Note that in the case of C<sub>2</sub> yield groups, each catalyst is assigned to a C<sub>2</sub> yield group according to the individual C<sub>2</sub> yield produced during the high throughput experiments (*e.g.* catalysts that produce C<sub>2</sub> yields that are less than 8% belong to the group “C<sub>2</sub> yield 0–8%”). Based on previous reports, cut-off points are based on catalyst-free OCM which produces a C<sub>2</sub> yield of 10% with a ±2% range for the “neutral” group (“C<sub>2</sub> yield 8–12%”).<sup>5</sup> C<sub>2</sub> yields that are less than 8% can be seen as yields that are negatively affected by catalytic activity while catalysts with C<sub>2</sub> yields greater than 12% can be seen as exhibiting higher degrees of catalytic activity. The preprocessed data are then transformed into an undirected graph through the Force Atlas 2 algorithm where node placement is influenced by how often nodes access other nodes (*e.g.* nodes that share many connections are closer to each other within the network).<sup>22</sup> Note that node sizes and colors are adjusted for visualization purposes.

Proposed catalysts are designed based on observations and information gathered from the catalyst networks illustrated in Fig. 1 and 2, in particular, elements that either clearly favor the C<sub>2</sub> yield group “C<sub>2</sub> yield 12+” or are found in grey areas between C<sub>2</sub> yield groups but are found to be closer to the C<sub>2</sub> yield group “C<sub>2</sub> yield 12+”. Additionally, element combinations are chosen based on how often certain element pairs appear near the C<sub>2</sub> yield group “C<sub>2</sub> yield 12+” and how likely they are to pair with particular supports.

## Results and discussion

### Creating an element/experimental condition network

High-throughput experimental data of catalysts used towards the OCM reaction are preprocessed and transformed into a network in order to analyze how various components of data relate to others. By visualizing the data as a network, it becomes possible to make several valuable observations about the catalyst that would otherwise be difficult to obtain when analyzing it in textual format. A network is generated from the collected and preprocessed data using Gephi where individual atomic elements of each catalyst are plotted with their corresponding supports, experimental conditions, and C<sub>2</sub> yields and can be found in Fig. 1. Catalysts are represented by their atomic elements and supports where each piece is listed individually. For instance, catalyst LiKMn–MgO is represented in the network as nodes “Li”, “K”, “Mn”, and “MgO”; thus, one catalyst





Fig. 1 Constructed network consisting of catalyst data with corresponding supports, experimental conditions, and C<sub>2</sub> yields. Nodes are colored as the following: atomic element (light green), support (dark green), CH<sub>4</sub> flow (blue), O<sub>2</sub> flow (red), Ar flow (brown), temperature (pink), CH<sub>4</sub>/O<sub>2</sub> ratio (purple), and C<sub>2</sub> yield group (yellow). Individual C<sub>2</sub> yields are listed by their value. Note that node sizes are adjusted for visualization purposes.

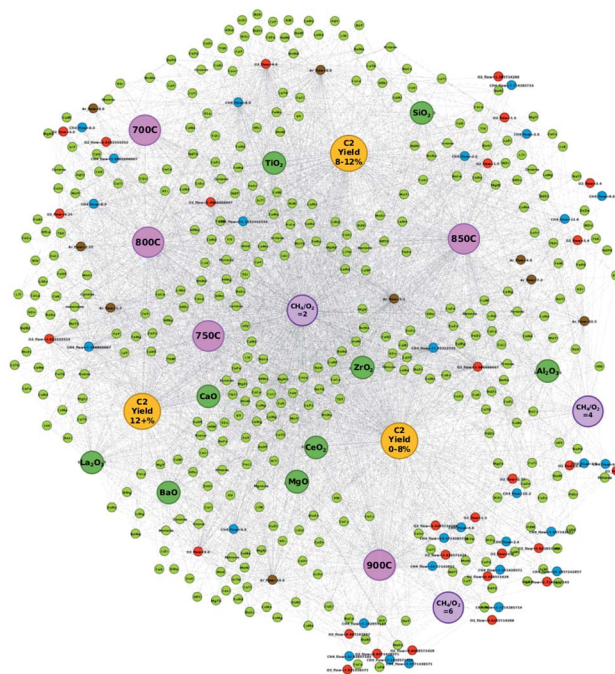


Fig. 2 Alternative constructed network consisting of catalyst data with corresponding supports, experimental conditions, and C<sub>2</sub> yields. Here, elements of the catalysts are represented as element pairs. Nodes are colored as follows: atomic element pair (light green), support (dark green), CH<sub>4</sub> flow (blue), O<sub>2</sub> flow (red), Ar flow (brown), temperature (pink), CH<sub>4</sub>/O<sub>2</sub> ratio (purple), and C<sub>2</sub> yield group (yellow). Note that node sizes are adjusted for visualization purposes.

is represented by four different nodes. By representing catalysts in this manner, it becomes possible to understand any possible trends present with atomic elements and supports such as tendencies to result in specific levels of catalytic activity or tendencies to pair with a subset of other atomic elements, supports, or particular experimental conditions. Nodes are also colored according to the type of information they represent as follows: atomic element (light green), support (dark green), CH<sub>4</sub> flow (blue), O<sub>2</sub> flow (red), Ar flow (brown), temperature (pink), CH<sub>4</sub>/O<sub>2</sub> ratio (purple), and C<sub>2</sub> yield group (yellow). Individual C<sub>2</sub> yields are listed by their value.

From Fig. 1, one can see that nodes representing individual atomic elements found within a catalyst can be found closer to some experimental conditions and C<sub>2</sub> yield groups rather than others. For example, atomic element nodes such as Pd and Cu are close to the C<sub>2</sub> yield group “C<sub>2</sub> yield 0–8%” while atomic element nodes such as Ti and Nd are close to the C<sub>2</sub> yield group “C<sub>2</sub> yield 8–12%”. This suggests that these elements have a clearer tendency to result in a particular range of catalytic activity, *e.g.* Pd and Cu tend to result in lower degrees of catalytic activity while Ti and Nd tend to result in a neutral level of catalyst activity when compared to the catalytic activity of other catalysts in this study. In the case of the C<sub>2</sub> yield group “C<sub>2</sub> yield 12+%”, it becomes less obvious where the boundaries between the C<sub>2</sub> yield groups lie. Their location between C<sub>2</sub> yield groups “C<sub>2</sub> yield 8–12%” and “C<sub>2</sub> yield 0–8%” results in many elements being placed in the shared spaces between “C<sub>2</sub> yield 0–8%” and “C<sub>2</sub> yield 12+%” and between C<sub>2</sub> yield groups “C<sub>2</sub> yield 0–8%”

and “C<sub>2</sub> yield 12+%”. Further analysis of the data reveals that atomic elements that fall within these grey areas between C<sub>2</sub> yield groups “C<sub>2</sub> yield 0–8%” and “C<sub>2</sub> yield 12+%” and between C<sub>2</sub> yield groups “C<sub>2</sub> yield 0–8%” and “C<sub>2</sub> yield 12+%” will result in varying levels of C<sub>2</sub> yields depending on their companion elements, supports, and experimental conditions. From this, one can understand that elements that fall within these so-called grey areas can be treated as elements whose catalytic performance is influenced by other elements or experimental conditions. Thus, the figure successfully illustrates the importance of combinatorial effects in the design of high-performance catalysts.

Fig. 1 also reveals that certain CH<sub>4</sub> flow, O<sub>2</sub> flow, and Ar flow conditions are found to closely associate with particular conditions. For instance, nodes representing the CH<sub>4</sub> flow, O<sub>2</sub> flow, and Ar flow tend to congregate around the nodes representing temperature. For example, CH<sub>4</sub> flows 6.0 and 11.33, O<sub>2</sub> flows 2.83 and 3.0, and Ar flow 6.0 are found in close proximity to the node representing “700 °C” and, as a set of conditions, are close to node “C<sub>2</sub> yield 8–12%”, this suggests that these particular experimental conditions are likely to be the conditions that elicit the best catalytic performance of the catalysts that fall within this range. Similarly, the network illustrates that the nodes representing gas flows tend to congregate around temperature nodes where particular temperatures will show closer proximity to certain C<sub>2</sub> yield groups. Given these observations, one can understand two points: (1) gas flows tend to



**Table 1** Proposed catalysts based on network information. Variables represent the following: A; element, B; support, C; temperature ( $^{\circ}\text{C}$ ), D;  $\text{CH}_4$  flow ( $\text{mL min}^{-1}$ ), E;  $\text{O}_2$  flow ( $\text{mL min}^{-1}$ ), F; Ar flow ( $\text{mL min}^{-1}$ ), G;  $\text{CH}_4/\text{O}_2$  ratio ( $\text{mol mol}^{-1}$ ), and H;  $\text{C}_2$  yield(%). Note that  $\text{C}_2$  yields correspond to the best yields when individual catalysts are tested under 135 sets of reaction conditions via high-throughput experiments

| A        | B                              | C   | D    | E   | F    | G  | H     |
|----------|--------------------------------|-----|------|-----|------|----|-------|
| TiKW     | BaO                            | 850 | 4    | 2   | 14   | 2  | 16.45 |
| TiCsW    | BaO                            | 850 | 4    | 2   | 14   | 2  | 17.45 |
| TiTbW    | BaO                            | 800 | 8    | 4   | 8    | 2  | 17.14 |
| SrHfnone | BaO                            | 850 | 4    | 2   | 14   | 2  | 15.01 |
| SrVnone  | BaO                            | 850 | 9.6  | 2.4 | 8    | 4  | 11.84 |
| SrHfMo   | BaO                            | 850 | 4    | 2   | 14   | 2  | 13.27 |
| SrMoW    | BaO                            | 900 | 4.8  | 2   | 14   | 2  | 13.54 |
| SrBaMo   | BaO                            | 850 | 4.8  | 1.2 | 14   | 4  | 16.81 |
| MoCsLi   | BaO                            | 850 | 4    | 2   | 14   | 2  | 17.39 |
| MoLiW    | BaO                            | 850 | 4    | 2   | 14   | 2  | 16.28 |
| MoVW     | BaO                            | 900 | 4.8  | 1.2 | 14   | 4  | 14.26 |
| MoKW     | BaO                            | 850 | 4    | 2   | 14   | 2  | 18.36 |
| MoCsZr   | BaO                            | 850 | 4    | 2   | 14   | 2  | 17.96 |
| CsZrW    | BaO                            | 800 | 4    | 2   | 14   | 2  | 17.32 |
| KVW      | BaO                            | 850 | 4.8  | 1.2 | 14   | 4  | 15.01 |
| VWMo     | BaO                            | 900 | 4.8  | 1.2 | 14   | 4  | 14.25 |
| KYMo     | BaO                            | 850 | 4    | 2   | 14   | 2  | 17.60 |
| KYV      | BaO                            | 850 | 4    | 2   | 14   | 2  | 18.21 |
| EuMgZr   | BaO                            | 800 | 8    | 4   | 8    | 2  | 18.82 |
| EuHfW    | ZrO <sub>2</sub>               | 850 | 8    | 4   | 8    | 2  | 8.05  |
| EuKW     | ZrO <sub>2</sub>               | 800 | 11.3 | 5.7 | 3    | 2  | 8.30  |
| BaEuW    | ZrO <sub>2</sub>               | 850 | 4    | 2   | 14   | 2  | 15.74 |
| EuVW     | ZrO <sub>2</sub>               | 850 | 11.3 | 5.7 | 3    | 2  | 8.32  |
| LiEuW    | ZrO <sub>2</sub>               | 800 | 4    | 2   | 4    | 2  | 14.16 |
| EuYW     | ZrO <sub>2</sub>               | 850 | 11.3 | 5.7 | 3    | 2  | 7.74  |
| EuCsW    | ZrO <sub>2</sub>               | 850 | 4    | 2   | 14   | 2  | 9.13  |
| EuMoW    | ZrO <sub>2</sub>               | 850 | 8    | 4   | 8    | 2  | 8.86  |
| EuLiW    | ZrO <sub>2</sub>               | 850 | 3    | 1.5 | 10.5 | 15 | 13.68 |
| KVW      | MgO                            | 800 | 6    | 3   | 6    | 2  | 8.47  |
| TiCeW    | TiO <sub>2</sub>               | 850 | 8    | 4   | 8    | 2  | 9.11  |
| TbHfW    | La <sub>2</sub> O <sub>3</sub> | 700 | 8    | 4   | 8    | 2  | 12.09 |
| TbTinone | CaO                            | 700 | 8    | 4   | 8    | 2  | 16.65 |

have share more connections with particular temperatures as seen by their congregation patterns, and (2) temperatures show more connections to some  $\text{C}_2$  yield groups over others. One can therefore treat these gas flow/temperature combinations as sets of conditions that have a stronger correlation with particular  $\text{C}_2$  yields.

While the development of the network illustrated in Fig. 1 helps clarify how different combinations of elements, supports, and experimental conditions relate to others, the combinations that result in  $\text{C}_2$  yields that fall under 8% become strikingly clear. Immediately, one can see that a temperature of  $900\text{ }^{\circ}\text{C}$  is strongly related to the  $\text{C}_2$  yield group “ $\text{C}_2$  yield 0–8%” along with  $\text{CH}_4/\text{O}_2$  ratios of 4 and 6. One can also see that a large array of  $\text{CH}_4$  flow and  $\text{O}_2$  flow nodes also exhibit a strong correlation with the  $\text{C}_2$  yield group “ $\text{C}_2$  yield 0–8%” along with atomic elements Cu, Pd, Zn, and Ni. Thus, the network better illustrates elements and supports that associate with conditions that correlate with low  $\text{C}_2$  yields and therefore it may be better to avoid them when designing high-performance catalysts.

Interestingly, transforming catalytic data into a network clarifies the outcomes of choosing different  $\text{CH}_4/\text{O}_2$  ratios. The location of the node representing the  $\text{CH}_4/\text{O}_2$  ratio of 2 within the network reflects how commonly this ratio is involved with the various types of catalysts, supports, and experimental conditions that were tested through high-throughput experimentation. Given its location at the center of the network, one can assume that this particular ratio does not show preference to any particular  $\text{C}_2$  yield outcome, thereby suggesting that other factors may be at play when determining  $\text{C}_2$  yields for the cases where the  $\text{CH}_4/\text{O}_2$  ratio of 2 is involved. Meanwhile,  $\text{CH}_4/\text{O}_2$  ratios of 6 and 4 are clearly close to the  $\text{C}_2$  yield group “ $\text{C}_2$  yield 0–8%”, suggesting that using these particular ratios when designing experiments to test catalysts will likely hinder catalytic performance.

Finally, by analyzing Fig. 1, several so-called “grey zones” are found to appear in areas between neighboring  $\text{C}_2$  yield groups. Various elements and experimental conditions are found in areas where they share equal or similar distances between more than one  $\text{C}_2$  yield group, suggesting that particular elements or experimental conditions may associate with a particular  $\text{C}_2$  yield group depending on the other elements, supports, and experimental conditions that they may be paired with. For instance, elements such as Sr or Cs can lead to  $\text{C}_2$  yields that fall within the  $\text{C}_2$  yield range of 8–12% or lead to a yield greater than 12% depending on what they are coupled with. Similarly, elements such as Zr, Mg, and Ba fall within a grey zone between  $\text{C}_2$  yield ranges of less than 8% and greater than 12%, suggesting that the elements' ability to invoke a higher  $\text{C}_2$  yield may depend on the elements or experimental conditions that they are partnered with. While these grey zones provide insights towards designing catalysts that result in higher  $\text{C}_2$  yields, the pairing effect that occurs between elements is still largely unknown.

From these results, it becomes clear that transforming catalytic data into a network provides a wealth of information regarding how various components affect the  $\text{C}_2$  yield of a given catalyst. Not only can one understand the likely  $\text{C}_2$  yield outcome of using different elements when designing a catalyst, but can also understand which experimental conditions can enhance the catalytic activity of the catalyst in question. Visualizing the data in this manner can therefore improve the efficiency of the catalyst design process and allow researchers to extract knowledge and apply it towards new catalysts and experimental designs.

### Analyzing the effect of element pairing

In order to better understand the effects of element pairing in relation to various experimental conditions and resulting  $\text{C}_2$  yields, the network is redesigned by representing element combinations as element pairs. The catalytic data are pre-processed in the same manner as previously discussed; however, catalysts are represented by the possible element pairs that can be made with the individual elements of the catalyst instead of individual atomic elements. For instance, catalyst  $\text{LiKMn-MgO}$ , which was previously represented in the network as nodes “Li”, “K”, “Mn”, and “MgO”, is now





Fig. 3 Locations of select elements (circled in black) within the catalyst network. Note that the circled elements are found within the proposed catalysts that resulted in  $C_2$  yields of 18% when validated via experiments.

represented as the following: “LiK”, “LiMn”, “KMn”, and “MgO”. By representing catalysts by their element pairs, the ability to design new catalysts that elicit a high  $C_2$  yield based on the network visualization becomes possible as it can potentially help clarify positive combinations of elements that may have otherwise fell within the “grey areas” between  $C_2$  groups as found in Fig. 1. This is in part due to how node placement is determined when constructing the network where node locations are determined by how frequently one piece of data accesses or is accessed by another piece of data within the dataset. By representing the elements of a catalyst as element pairs, it becomes easier to determine which element combinations will likely result in high or low  $C_2$  yields. Supports,  $CH_4$  flow,  $O_2$  flow, Ar flow,  $CH_4/O_2$  ratios (2, 4, and 6), temperatures (700 °C, 750 °C, 800 °C, 850 °C, and 900 °C), and  $C_2$  yield groups “ $C_2$  yield 0–8%”, “ $C_2$  yield 8–12%”, and “ $C_2$  yield 12+%” are also defined as nodes. Nodes are also colored according to the type of information they represent and are colored as the following: atomic element pair (light green), support (dark green),  $CH_4$  flow (blue),  $O_2$  flow (red), Ar flow (brown), temperature (pink),  $CH_4/O_2$  ratio (purple), and  $C_2$  yield group (yellow). Edges represent the connections shared between two nodes while the edge weight is set to 1. For the new network, individual  $C_2$  yield values are excluded in order to focus on the element pair nodes.

Fig. 2 illustrates the new network where elements within a catalyst are represented as their possible pairs. For instance, elements of catalyst LiEuW– $ZrO_2$  would be represented as LiEu, LiW, and EuW, respectively, while its support  $ZrO_2$  is represented separately. By representing the elements in this manner, the pairing effect becomes clearer. For instance, in Fig. 1, element Ba is located within a grey zone between yield

groups “ $C_2$  yield 12+%” and “ $C_2$  yield 0–8%”. However, when represented as pairs, one can see that element pair BaEu correlates more with the yield group “ $C_2$  yield 12+%” than with the  $C_2$  yield group “ $C_2$  yield 0–8%”. Cases like W also prove to be interesting when comparing the location of nodes between networks. In Fig. 1, the node representing W is found to be closely related to the yield group “ $C_2$  yield 12+%”. In Fig. 2, W is found to be much more closely related to the yield group “ $C_2$  yield 12+%” when paired with elements such as Cs, Mo, Hf, and Li. Meanwhile, W more closely relates to the yield group “ $C_2$  yield 0–8%” when paired with elements Pd and Sr. This therefore illustrates that the catalytic performance of elements is affected by the elements they are paired with, which can improve or worsen the catalytic activity of the catalyst.

Representing elements in this manner also helps dispel preheld ideas that particular elements are considered to be poor. As seen in Fig. 1, the element Pd is strongly associated with the  $C_2$  yield group “ $C_2$  yield 0–8%”; however, Fig. 2 illustrates that Pd, when paired with Ti, Ba, or Co, is found to be much more closely associated with the  $C_2$  yield group “ $C_2$  yield 8–12%”. The elements Ti, Ba, and Co, in the meantime, are positioned near the  $C_2$  yield group “ $C_2$  yield 8–12%” or within the grey zone between  $C_2$  yield groups “ $C_2$  yield 12+%” and “ $C_2$  yield 0–8%”. This suggests that elements that may be considered to traditionally have poor catalytic performance could potentially be improved by pairing with elements that are typically viewed as having good catalytic performance. Furthermore, the network in Fig. 2 helps clarify ambiguity regarding elements that fall within the grey zones between the  $C_2$  yield groups in Fig. 1. Thus, by looking at these networks, it becomes possible to design new element combinations that





Fig. 4 Locations of element pairs (circled in black) for catalysts EuMgZr–BaO, MoKW–BaO, and KYV–BaO, which are found to have a C<sub>2</sub> yield of 18%.

may result in C<sub>2</sub> yields higher than 12% by combining elements and experimental conditions that fall within the vicinity of the C<sub>2</sub> yield group “C<sub>2</sub> yield 12+%”.

#### Testing designed catalysts based on network visualization

In order to test the efficiency of designing catalysts based on network visualization, 32 catalyst combinations are designed



and then tested *via* high-throughput experiments. Atomic element combinations and potential experimental conditions are proposed using the networks illustrated in Fig. 1 and 2. A glance at Fig. 1 shows that atomic elements such as W, Li, K, Mo, and La strongly associate with the C<sub>2</sub> yield group “C<sub>2</sub> yield 12+%” while atomic elements such as Ca, V, Mn, and Tb are found in a grey area between C<sub>2</sub> yield groups “C<sub>2</sub> yield 8–12%” and “C<sub>2</sub> yield 12+%”. Given that these elements are involved in designing catalysts that result in various C<sub>2</sub> yields, a more detailed network like the one shown in Fig. 2 becomes necessary in order to pinpoint element combinations that potentially result in a desired outcome like high C<sub>2</sub> yield.

An initial glance at Fig. 2 shows that supports BaO, CaO, and La<sub>2</sub>O<sub>3</sub> are strongly associated with the C<sub>2</sub> yield group “C<sub>2</sub> yield 12+%”, suggesting that these supports have a higher likelihood of resulting in C<sub>2</sub> yields when used experimentally. From there, element combinations that are found close to these supports are analyzed. Closer analysis of Fig. 2 shows that element W, which is found to strongly associate with the C<sub>2</sub> yield group “C<sub>2</sub> yield 12+%” in Fig. 1, is also found to be paired with elements that correlate with the C<sub>2</sub> yield group “C<sub>2</sub> yield 12+%”. Similar observations are made for elements such as Ca and Tb with pairs such as CaK, CaTi, CaNd, FeTb, MoTb, and TbTi. By listing the atomic elements according to the additional atomic elements they are paired with, it becomes easier to understand which particular combinations of elements may result in a higher C<sub>2</sub> yield. This can help clarify cases where atomic elements fall within grey zones as the element pairs can clarify which particular combinations of elements will fall under different C<sub>2</sub> yield groups.

Designing catalysts according to node placements within the networks is further investigated in order to determine the accuracy and efficiency of designing catalysts in this manner. Table 1 lists the first batch of catalysts predicted with this method. Catalysts are designed based on the information visualized in Fig. 1 and 2. Fig. 1 is used to select elements that clearly favor the C<sub>2</sub> yield group “C<sub>2</sub> yield 12+%” or are found in grey areas between C<sub>2</sub> yield groups but also show affinity for “C<sub>2</sub> yield 12+%”. Fig. 2 is used to not only find combinations of these elements that fall within the vicinity of the C<sub>2</sub> yield group “C<sub>2</sub> yield 12+%” as seen in Fig. 1, but also search for any elements that are observed in a sizeable number of element pairs within the “C<sub>2</sub> yield 12+%” range. Also, element combinations are chosen based on elements that are found to be common in element pairs near a particular support.

The catalysts suggested in Table 1 are tested experimentally. Out of the suggested elemental combinations, 23 cases result in a C<sub>2</sub> yield that can be categorized as “C<sub>2</sub> yield 12+%”, 8 cases result in a C<sub>2</sub> yield that can be categorized as “C<sub>2</sub> yield 8–12%”, and 1 case results in a C<sub>2</sub> yield that can be categorized as “C<sub>2</sub> yield 0–8%”. From this, one can see that over half of the suggested elemental combinations result in high C<sub>2</sub> yields; more specifically, 70% of the catalysts produced a C<sub>2</sub> yield of 12% or greater when tested *via* high throughput experiments. In particular, catalysts EuMgZr–BaO, MoKW–BaO, and KYV–BaO result in C<sub>2</sub> yields (%) of 18.82, 18.36, and 18.21, respectively, while catalysts MoCsZr–BaO, KYMO–BaO, TiCsW–BaO,

Table 2 Proposed catalysts of Table 1 represented by their element pairs

| Proposed catalyst                    | Element pair 1 | Element pair 2 | Element pair 3 |
|--------------------------------------|----------------|----------------|----------------|
| EuMgZr–BaO                           | EuMg           | EuZr           | MgZr           |
| MoKW–BaO                             | MoK            | MoW            | KW             |
| KYV–BaO                              | KY             | KV             | VY             |
| MoCsZr–BaO                           | MoCs           | MoZr           | CsZr           |
| KYMO–BaO                             | KY             | KMo            | KMo            |
| TiCsW–BaO                            | TiCs           | TiW            | TiW            |
| MoCsLi–BaO                           | MoCs           | MoLi           | CsLi           |
| CsZrW–BaO                            | CsZr           | CsW            | ZrW            |
| TiTbW–BaO                            | TiTb           | TiW            | TbW            |
| SrBaMo–BaO                           | SrBa           | SrMo           | BaMo           |
| TbTi–CaO                             | TbTi           | Tb             | Ti             |
| TKW–BaO                              | TK             | TW             | KW             |
| MoLiW–BaO                            | MoLi           | MoW            | LiW            |
| BaEuW–ZrO <sub>2</sub>               | BaEu           | BaW            | EuW            |
| SrHf–BaO                             | SrHf           | Sr             | Hf             |
| KVW–BaO                              | KV             | KW             | VW             |
| MoVW–BaO                             | MoV            | MoW            | VW             |
| LiEuW–ZrO <sub>2</sub>               | LiEu           | LiW            | EuW            |
| EuLiW–ZrO <sub>2</sub>               | EuLi           | EuW            | LiW            |
| SrMoW–BaO                            | SrMo           | SrW            | MoW            |
| SrHfMo–BaO                           | SrHf           | SrMo           | HfMo           |
| TbHfW–La <sub>2</sub> O <sub>3</sub> | TbHf           | TbW            | HfW            |
| KVW–MgO                              | KV             | KW             | VW             |
| SrV–BaO                              | SrV            | Sr             | V              |
| EuCsW–ZrO <sub>2</sub>               | EuCs           | CsW            | CsW            |
| TiCeW–TiO <sub>2</sub>               | TiCe           | TiW            | CeW            |
| EuMoW–ZrO <sub>2</sub>               | EuMo           | EuW            | MoW            |
| EuVW–ZrO <sub>2</sub>                | EuV            | EuW            | VW             |
| EuKW–ZrO <sub>2</sub>                | EuK            | EuW            | KW             |
| EuHfW–ZrO <sub>2</sub>               | EuHf           | EuW            | HfW            |
| EuYW–ZrO <sub>2</sub>                | EuY            | EuW            | YW             |

MoCsW–BaO, CsZrW–BaO, and TiTbW–BaO resulted in C<sub>2</sub> yields (%) of 17.96, 17.60, 17.45, 17.39, 17.32, and 17.14, respectively. One can therefore understand that using the constructed network to represent catalysts and experimental conditions with their respective yields can help increase the likelihood of designing a catalyst with higher C<sub>2</sub> yields.

The elements of these catalysts are compared against their locations within the created networks in order to better understand the reliability of network-based catalyst design. To start with, the elements that make up the catalysts that result in C<sub>2</sub> yields of 18% – Eu, Mg, Zr, Mo, K, W, Y, and V – are highlighted in Fig. 3 which shows that these elements often fall within a grey area found between C<sub>2</sub> yield groups “C<sub>2</sub> yield 12+%” and “C<sub>2</sub> yield 0–8%”. Elements that make up the catalysts that result in C<sub>2</sub> yields of 17% – Mo, Cs, Zr, K, Y, Ti, W, Li, and Tb – are also not only found within the grey areas between C<sub>2</sub> yield groups “C<sub>2</sub> yield 12+%” and “C<sub>2</sub> yield 0–8%”, but in some cases are also between C<sub>2</sub> yield groups “C<sub>2</sub> yield 12+%” and “C<sub>2</sub> yield 8–12%”. From this, one can come to the understanding that the efficiency of these elements is affected by the elements that they are paired with.

Fig. 4 illustrates where these elements can be found in relation to the C<sub>2</sub> yield groups when represented by their element pairs as listed in Table 2. By representing the data in



**Table 3** Second batch of proposed catalysts. Variables represent the following: A; element, B; support, C; temperature ( $^{\circ}\text{C}$ ), D;  $\text{CH}_4$  flow ( $\text{mL min}^{-1}$ ), E;  $\text{O}_2$  flow ( $\text{mL min}^{-1}$ ), F; Ar flow ( $\text{mL min}^{-1}$ ), G;  $\text{CH}_4/\text{O}_2$  ratio ( $\text{mol mol}^{-1}$ ), H;  $\text{C}_2$  yield(%). Note that experimental  $\text{C}_2$  yields are in reference to  $\text{C}_2$  yields produced when the catalysts are tested *via* high-throughput experiments

| A      | B   | C   | D     | E    | F  | G | H     |
|--------|-----|-----|-------|------|----|---|-------|
| KVEu   | BaO | 850 | 4     | 2    | 14 | 2 | 20.38 |
| VMoEu  | BaO | 850 | 4     | 2    | 14 | 2 | 16.96 |
| KCaMo  | BaO | 800 | 4     | 2    | 14 | 2 | 18.23 |
| KVZr   | BaO | 850 | 4     | 2    | 14 | 2 | 14.8  |
| MgZrCs | BaO | 800 | 4     | 2    | 14 | 2 | 15.16 |
| MgYZr  | BaO | 850 | 4     | 2    | 14 | 2 | 18.62 |
| KVY    | CaO | 750 | 11.33 | 5.67 | 3  | 2 | 11.94 |
| KYMo   | CaO | 750 | 8     | 4    | 8  | 2 | 11.49 |
| LiTiW  | BaO | 850 | 4     | 2    | 14 | 2 | 19.03 |

this manner, the particular pairs of elements that result in high  $\text{C}_2$  yields become clearer. For instance, in the case of proposed catalyst “EuMgZr–BaO”, the element pair “EuMg” is found closer to the  $\text{C}_2$  yield group “ $\text{C}_2$  yield 0–8%” while element pairs “MgZr” and “EuZr” are found closer to the  $\text{C}_2$  yield group “ $\text{C}_2$  yield 12+%” and in the grey area between groups “ $\text{C}_2$  yield 12+%” and “ $\text{C}_2$  yield 0–8%”, respectively. Here, one can see that while “EuMg” may be more associated with catalysts that result in  $\text{C}_2$  yields that are low, their combination with element Zr improves the  $\text{C}_2$  yield (as seen by the placements of “MgZr” and “EuZr”). This effect is also seen with proposed catalysts MoKW–BaO and KYV–BaO, where element pairs “MoK” and “VY” share

association with the  $\text{C}_2$  yield group “ $\text{C}_2$  yield 8–12%” and the remaining element pairs are found near the  $\text{C}_2$  yield group “ $\text{C}_2$  yield 12+%”. By studying the locations of these element pairs, it becomes possible to not only improve the efficiency of a designed catalyst by choosing element combinations that strongly associate with high  $\text{C}_2$  yields but also can potentially improve the efficiency of catalysts with poor performance by selectively replacing elements with other elements that result in higher catalytic performance.

A second batch of catalysts are then proposed and are presented in Table 3. Combinations are chosen based on observations made with previous results to explore element combinations that were not initially present in the data. Out of the second set of proposed catalysts, 7 are found to produce  $\text{C}_2$  yields that fall within the category of “ $\text{C}_2$  yield 12+%” while the remaining two produce  $\text{C}_2$  yields that fall within the category “ $\text{C}_2$  yield 8–12%”. No catalysts produce yields that would fall within the  $\text{C}_2$  yield category “ $\text{C}_2$  yield 0–8%”. Thus, one can see that using the created networks to design catalysts in an informed manner can help decrease time and resources spent on catalyst development and testing while also have a higher chance of successfully returning a  $\text{C}_2$  yield that is considered to be high.

Catalysts KVEu–BaO and LiTiW–BaO are also found to elicit  $\text{C}_2$  yields of 20.38% and 19.03%, respectively, which outperform those of the remaining proposed catalysts and have also not been previously reported. Further analysis is conducted in order to better understand why these combinations may have resulted in such high yields. Fig. 5 illustrates the element pair nodes for proposed catalyst KVEu–BaO that share connections with the



**Fig. 5** Element pair nodes for proposed catalyst KVEu–BaO and experimental condition nodes that they relate to.



nodes for the experimental conditions. Here, one can see that the element pair nodes EuV, KV, and EuK share connections with supports and other experimental conditions that fall around the C<sub>2</sub> yield groups “C<sub>2</sub> yield 12+%” and “C<sub>2</sub> yield 0–8%”. Given that the element pair nodes are located in the grey area between the two C<sub>2</sub> yield groups, it is likely that the success of these elements is in some way dependent on the supports and gas flows that accompany them. For instance, supports BaO and CaO are seen to have a strong correlation with the C<sub>2</sub> yield group “C<sub>2</sub> yield 12+%” while support CeO<sub>2</sub> strongly correlates with “C<sub>2</sub> yield 0–8%”. A similar effect is also seen with LiTiW–BaO, where element pairs LiTi and TiW are seen near the C<sub>2</sub> yield group “C<sub>2</sub> yield 8–12%” and LiW is found within the grey area between C<sub>2</sub> yield groups “C<sub>2</sub> yield 12+%” and “C<sub>2</sub> yield 0–8%”. Interestingly, the network did not include a case where any of these element pairs are connected with the support BaO. Given that the node for support BaO correlates strongly with the C<sub>2</sub> yield group “C<sub>2</sub> yield 12+%”, it is reasonable to believe that pairing the mid-level performing elements with a potentially high-level performing element with a support like BaO can improve the catalytic performance of the proposed catalyst. Further studies, however, are required in order to determine the long-term stability of these catalysts. These results thereby show that targeted design of new catalysts can be carried out more efficiently with the relational information that can be extracted through studying a network representation of catalytic data.

## Conclusion

Transforming catalyst data generated from high-throughput experiments into networks has proven to be beneficial in several ways. To start with, by visualizing the transformation of catalyst data into networks, it becomes easier to understand correlations between atomic elements, their supports, and corresponding experimental conditions in relation to C<sub>2</sub> yields produced during the OCM reaction. One can see that elements either have clear associations with a particular C<sub>2</sub> yield group or are found in areas between groups, which suggests that the performance of these so-called “grey-area” elements is influenced by other factors such as the elements they are paired with or other experimental factors such as temperature. The pairing effect of elements on the performance of catalysts is easier to understand when the data are retransformed into a network where catalysts are represented by their possible element pairs. Thirty-two catalysts are then designed using the constructed networks and then tested *via* high-throughput experiments with the aim of producing catalysts that result in high C<sub>2</sub> yields during the OCM process. Out of the 32 catalysts, 23 are found to result in C<sub>2</sub> yields greater than 12%, with 9 catalysts resulting in C<sub>2</sub> yields of 17% or greater. Further analysis of these catalysts shows that elements that are found in grey areas are improved by elements that had correlations with high yield-producing catalysts, thereby demonstrating that catalyst performance can be enhanced through deliberate elemental pairings. Additional catalysts are designed and tested in order to confirm the efficiency of catalyst design *via* a network, where 7 out of the 9 catalysts are found to have C<sub>2</sub> yields greater than 12%. Two

catalysts in particular – KVEU–BaO and LiTiW–BaO – are found to elicit C<sub>2</sub> yields of 20.38% and 19.03% and have not been previously reported, though long-term stability requires further investigation. Catalyst knowledge networks provide a way to design catalysts based on the relationships provided by catalyst data. In particular, this enables the ability to design highly active OCM catalysts. One can consider that the networks can assist further developments of catalysts, *e.g.* through doping or optimization of composition ratios, by providing information that could potentially lead to the enhancement of catalytic activity. If catalyst big data contains doping and ratio of composition information of catalysts, a further detailed catalyst knowledge network can, in principle, be developed. Thus, by creating networks of catalysts and experimental conditions of data produced *via* high-throughput experiments, catalysts with high performance can be designed in a much more efficient manner with a higher likelihood of success than traditional methods used during the catalyst design process.

## Data availability

Data used to construct the networks presented in Fig. 1 and 2 have been uploaded as part of the ESI.†

## Author contributions

LT and KT conceived the idea for this analysis, determined methodologies, and wrote and reviewed the published work. LT curated catalyst data and applied network-related methods for formal analysis and visualization. TNN, SN, and AF tested designed catalysts in experiment. TT reviewed the published work and provided resources for experimental investigations. KT acquired funding for this published work.

## Conflicts of interest

There are no conflicts of interest to declare.

## Acknowledgements

This work is funded by Japan Science and Technology Agency (JST) CREST Grant Number JPMJCR17P2.

## Notes and references

- 1 J. K. Nørskov and T. Bligaard, The Catalyst Genome, *Angew. Chem.*, 2013, **52**, 776–777.
- 2 J. K. Nørskov, T. Bligaard, J. Rossmeisl and C. H. Christensen, Towards the Computational Design of Solid Catalysts, *Nat. Chem.*, 2009, **1**, 37.
- 3 A. J. Medford, M. R. Kunz, S. M. Ewing, T. Borders and R. Fushimi, Extracting Knowledge from Data Through Catalysis Informatics, *ACS Catal.*, 2018, **8**, 7403–7429.
- 4 T. N. Nguyen, T. T. P. Nhat, K. Takimoto, A. Thakur, S. Nishimura, J. Ohyama, I. Miyazato, L. Takahashi, J. Fujima, K. Takahashi and T. Taniike, High-Throughput



- Experimentation and Catalyst Informatics for Oxidative Coupling of Methane, *ACS Catal.*, 2020, **10**, 921–932.
- 5 T. N. Nguyen, S. Nakanowatari, T. P. Nhat Tran, A. Thakur, L. Takahashi, K. Takahashi and T. Taniike, Learning Catalyst Design Based on Bias-Free Data Set for Oxidative Coupling of Methane, *ACS Catal.*, 2021, **11**, 1797–1809.
- 6 S. Nakanowatari, T. N. Nguyen, H. Chikuma, A. Fujiwara, K. Seenivasan, A. Thakur, L. Takahashi, K. Takahashi and T. Taniike, Extraction of catalyst design heuristics from random catalyst dataset and their utilization in catalyst development for oxidative coupling of methane, *ChemCatChem*, 2021, **13**(14), 3262–3269.
- 7 U. Zavyalova, M. Holena, R. Schlögl and M. Baerns, Statistical Analysis of Past catalytic Data on Oxidative Methane Coupling for New Insights into the Composition of High-performance Catalysts, *ChemCatChem*, 2011, **3**, 1935–1947.
- 8 J. R. Kitchin, Machine learning in catalysis, *Nat. Catal.*, 2018, **1**, 230–232.
- 9 P. Schlexer Lamoureux, K. T. Winther, J. A. Garrido Torres, V. Streibel, M. Zhao, M. Bajdich, F. Abild-Pedersen and T. Bligaard, Machine Learning for Computational Heterogeneous Catalysis, *ChemCatChem*, 2019, **11**, 3581–3601.
- 10 K. Takahashi, L. Takahashi, I. Miyazato, J. Fujima, Y. Tanaka, T. Uno, H. Satoh, K. Ohno, M. Nishida and K. Hirai, The Rise of Catalyst Informatics: Towards Catalyst Genomics, *ChemCatChem*, 2019, **11**, 1146–1152.
- 11 K. Suzuki, T. Toyao, Z. Maeno, S. Takakusagi, K.-i. Shimizu and I. Takigawa, Statistical analysis and discovery of heterogeneous catalysts based on machine learning from diverse published data, *ChemCatChem*, 2019, **11**, 4537–4547.
- 12 S. A. Palkovits, Primer about Machine Learning in Catalysis—A Tutorial with Code, *ChemCatChem*, 2020, **12**, 3995–4008.
- 13 S. Mine, M. Takao, T. Yamaguchi, T. Toyao, Z. Maeno, S. Siddiki, S. Takakusagi, K.-i. Shimizu and I. Takigawa, Analysis of Updated Literature Data up to 2019 on the Oxidative Coupling of Methane Using an Extrapolative Machine-Learning Method to Identify Novel Catalysts, *ChemCatChem*, 2021, **13**(16), 3636–3655.
- 14 E. N. Voskresenskaya, V. G. Roguleva and A. G. Anshits, Oxidant activation over structural defects of oxide catalysts in oxidative methane coupling, *Catal. Rev.*, 1995, **37**, 101–143.
- 15 S.-f. Ji, T.-c. Xiao, S.-b. Li, C.-z. Xu, R.-l. Hou, K. S. Coleman and M. L. Green, The relationship between the structure and the performance of Na-W-Mn/SiO<sub>2</sub> catalysts for the oxidative coupling of methane, *Appl. Catal., A*, 2002, **225**, 271–284.
- 16 Z. W. Ulissi, A. J. Medford, T. Bligaard and J. K. Nørskov, To address surface reaction network complexity using scaling relations machine learning and DFT calculations, *Nat. Commun.*, 2017, **8**, 1–7.
- 17 R. Schmack, A. Friedrich, E. V. Kondratenko, J. Polte, A. Werwatz and R. Kraehnert, A meta-analysis of catalytic literature data reveals property-performance correlations for the OCM reaction, *Nat. Commun.*, 2019, **10**, 1–10.
- 18 L. Takahashi and K. Takahashi, Visualizing Scientists' Cognitive Representation of Materials Data through the Application of Ontology, *J. Phys. Chem. Lett.*, 2019, **10**, 7482–7491.
- 19 G. Keller and M. Bhasin, Synthesis of Ethylene via Oxidative Coupling of Methane: I. Determination of Active Catalysts, *J. Catal.*, 1982, **73**, 9–19.
- 20 A. Galadima and O. Muraza, Revisiting the Oxidative Coupling of Methane to Ethylene in the Golden Period of Shale Gas: A Review, *J. Ind. Eng. Chem.*, 2016, **37**, 1–13.
- 21 M. Bastian, S. Heymann and M. Jacomy, Gephi: an Open Source Software for Exploring and Manipulating Networks, *Icwm*, 2009, **8**, 361–362.
- 22 M. Jacomy, T. Venturini, S. Heymann and M. Bastian, ForceAtlas2, a continuous graph layout algorithm for handy network visualization designed for the Gephi software, *PloS One*, 2014, **9**, e98679.
- 23 J. H. Lunsford, The Catalytic Oxidative Coupling of Methane, *Angew. Chem.*, 1995, **34**, 970–980.

